Chinese Chemical Letters 32 (2021) 2021–2026

Contents lists available at ScienceDirect

Chinese Chemical Letters

journal homepage: www.elsevier.com/locate/cclet

Communication

MXene-composited highly stretchable, sensitive and durable hydrogel for flexible strain sensors

Wei Yuan[a], Xinyu Qu[a], Yao Lu[a], Wen Zhao[a], Yanfang Ren[b], Qian Wang[a,*], Wenjun Wang[b], Xiaochen Dong[a,c,*]

[a] Key Laboratory of Flexible Electronics (KLOFE) & Institute of Advanced Materials (IAM), School of Physical and Mathematical Sciences, Nanjing Tech University (NanjingTech), Nanjing 211800, China
[b] School of Physical Science and Information Technology, Liaocheng University, Liaocheng 252059, China
[c] School of Chemistry and Materials Science, Nanjing University of Information Science & Technology, Nanjing 210044 China

ARTICLE INFO

Article history:
Received 24 July 2020
Received in revised form 20 August 2020
Accepted 6 December 2020
Available online 11 December 2020

Keywords:
Hydrogel
MXene
Strain sensor
High stretchablity and sensitivity
Durability

ABSTRACT

The flourishing development in flexible electronics has provoked intensive research in flexible strain sensors to realize accurate perception acquisition under different external stimuli. However, building hydrogel-based strain sensors with high stretchability and sensitivity remains a great challenge. Herein, MXene nanosheets were composited into polyacrylamide-sodium alginate matrix to construct mechanical robust and sensitive double networked hydrogel strain sensor. The hydrophilic MXene nanosheets formed strong interactions with the polymer matrix and endowed the hydrogel with excellent tensile properties (3150%), compliant mechanical strength (2.03 kPa^{-1} in Young's Module) and long-lasting stability and fatigue resistance (1000 dynamic cycles under 1,600% strain). Due to the highly oriented MXene-based three dimensional conductive networks, the hydrogel sensor achieved extremely high tensile sensitivity (18.15 in gauge factor) and compression sensitivity (0.38 kPa^{-1} below 3 kPa). MXene hydrogel-based strain sensors also displayed negligible hysteresis in electromechanical performance, typical frequent-independent feature and rapid response time to external stimuli. Moreover, the sensor exhibited accurate response to different scales of human movements, providing potential application in speech recognition, expression recognition and handwriting verification.

In the fields of wearable devices, medical electronics and intelligent robots [1–3], the applications of conventional sensors, made of rigid semiconductor materials or metal materials [4–6], are severely impeded by the limited flexibility and mechanical compliance. Flexible sensors, with high stretchability and robust mechanical strength, have gradually received extensive attention in flexible electronic devices. Hydrogel, a polymer porous network structure with high content of water, features excellent hydrophilicity, stretchability and mechanical compliance, and have widely emerged in fields of drug delivery [7,8], wound dressings [9] and energy storage [10,11]. By incorporating specific functional groups into the polymer network, properties of self-healing [12–14], shape-memory [15] and anti-freezing [16,17], *etc.*, can also be endowed to fulfill the requirements at different circumstances. However, it remains a great challenge to combine the high stretchablity and high sensitivity in a hydrogel strain sensor for practical sensing applications, which demands maintaining the integrity of the overall polymer matrix under large deformation and revealing violent changes in the conductive network under small deformation simultaneously.

Methods have been proposed quantitatively to enhance the mechanical and electrical performance of hydrogels. A double network structure, with different kinds of chemical and physical interactions in the polymer matrix, would break the "sacrificial bond" and release the local stress to alleviate stress concentration, improving the stretchability of the hydrogel. The mechanical property can also be enhanced by compositing nanomaterials fillers into the polymer network by providing alternative energy dissipating paths [18,19]. Currently, perceptual materials, such as nanoparticles, nanowires and carbon-based materials have been widely introduced into polymer networks to improve the stretchability and sensitivity of strain sensor synchronously. Thereinto, two-dimensional (2D) conductive nanomaterials, for

* Corresponding authors at: Key Laboratory of Flexible Electronics (KLOFE) & Institute of Advanced Materials (IAM), School of Physical and Mathematical Sciences, Nanjing Tech University (NanjingTech), Nanjing 211800, China.
E-mail addresses: chelseawq@njtech.edu.cn (Q. Wang), iamxcdong@njtech.edu.cn (X. Dong).

https://doi.org/10.1016/j.cclet.2020.12.003
1001-8417/

example, graphene and its derivatives [20–23], black phosphorus [24], have attracted intensive attention due to their unique properties of flexibility, plane covalent bonding and mechanical reliance and strength.

The newly developed 2D laminated transition metal carbide, MXene (Ti_3C_2), with extrusive hydrophobicity, high electrical conductivity and chemical stability, has provoked in the hydrogels for flexible electronic devices. The surface of MXene nanosheets treated with hydrofluoric acid exposes large numbers of active hydrogen bonds and functional groups (−OH, −F, −O) [25]. The highly hydrophilic MXene nanosheets can be uniformly dispersed in the hydrogel without accumulation and stacking, avoiding stress concentration and microcrack proliferation under external stimuli [26]. In addition, the large specific surface area and hydrogen bonding also enable strong interface interaction between MXene nanosheets and polymer matrix, endowing the hydrogel with enhanced mechanical strength [26]. Moreover, with high electrical conductivity [27,28], MXene nanosheets build up a continuous conductive network throughout the polymer matrix and ensures violent resistance change under external stain, showing apparent improvement on the sensitivity of the hydrogel. With enhancement in electromechanical performance, MXene nanosheets shows promising prospect to improve the mechanical strength, stretchability and sensitivity in hydrogel flexible sensors compared with some carbon nanomaterials. For example, Zhang et al. has incorporated MXene nanosheets into crystal clays to achieve a hydrogel with impressive stretchablity of 2200% strain and tensile strain sensitivity with a gauge factor (GF) of 25 [29]. Approaches are still under promotion to achieve hydrogel strain sensor with excellent electromechanical performance and high durability to external stimuli.

In this work, we synthesized and crosslinked Ti_3C_2 MXene with acrylamide (AM) and sodium alginate (SA) to form double network hydrogel strain sensor. The content of MXene and SA were valued to assess their influence on the mechanical strength of the hydrogel. The as-prepared MXene composited hydrogel displayed high stretchability and cyclic stability to external stimuli. The hydrogel strain sensor also exhibited impressive sensitivity and rapid response time to both tension and compression, enabling their promising application in different scales of human movement detection, phonetic recognition and handwriting verification. MXene was firstly prepared by a high temperature etching method, as have been reported previously [30]. The aluminum layer in Ti_3AlC_2 was etched in a mixed solution of HCl and HF at 180 °C and the single-layered Ti_3C_2 nanosheets were achieved (Fig. S1 in Supporting information). In the X-ray diffraction (XRD) patterns in Fig. 1a, most peaks of the MAX (Fig. 1a) weakened or disappeared after HF etching, and typical characteristic peak appeared at 6.7° for MXene, which can be well indexed to (000 l) plane of Ti_3C_2, indicating that the MAX phase has converted into MXene [30]. As displayed in Fig. 1b, the size of the obtained ultrathin MXene nanoplatelets ranges from 400 nm to 800 nm and exhibits high aspect ratio.

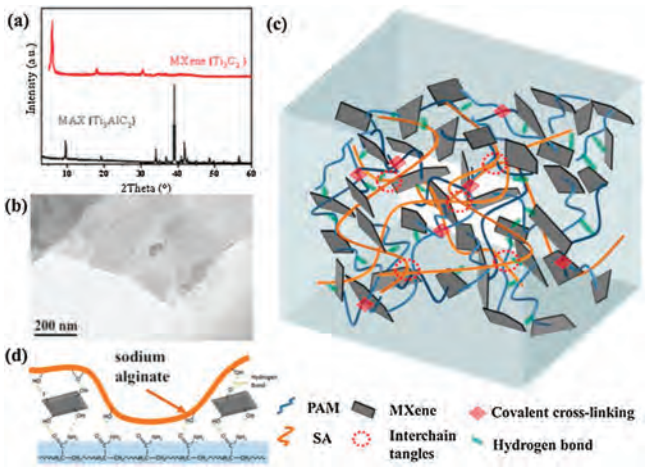

Fig. 1. (a) XRD patterns and (b) transmission electron microscopy image of MXene. (c) MXene-based hydrogel network diagram. (d) Description of hydrogen bonding between MXene and PAM, SA and covalent cross-linking of PAM chains.

The MXene-composited hydrogel was prepared by dispersing the MXene nanosheets in a polymer skeleton of polyacrylamide (PAM) and SA to fabricate three-dimensional (3D) conductive matrix. The detailed materials and synthesis process were illustrated in the Supporting information. Fig. 1c schematically sketches the network structure in the hydrogel. The AM monomers covalently crosslink into PAM long chains to provide a stretchable and resilient network, and the strong physical interaction among PAM, MXene and SA forms substantial hydrogen bonding, structuring a double-networked 3D conductive polymer network [31]. Fig. 1d gives a detailed description of the chemical and physical bonding in the matrix: the amide groups in PAM bond with the hydroxyl groups in SA to form the double-networked hydrogel, and MXene nanosheets, with sufficient hydrophilic terminal functional groups on the surface, build strong interactions both with the PAM and SA chains to reinforce the polymer matrix, enabling the hydrogel with high stretchability and mechanical robustness.

In the dual network, the long chain SA randomly entangles with the PAM and forms hydrogen bonds with the adjacent long chain, and the "sacrificed bond" could effectively dissipate energy to improve the stretchability of the double-networked hydrogel [32,33]. Herein, the tensile property of the SA-PAM hydrogel with different SA contents of 0, 0.5, 1 and 1.5 wt% are displayed in Fig. 2a. It is demonstrated that the added SA significantly improves the stretchability of the SA-PAM hydrogels, and the critical stretch varies with the SA content. When the content of SA increase to 1%, the critical stretch reaches the highest 860%. It suggests that the synergy effect of the dual network can greatly enhance the stretchability of the hydrogel with rapid energy dissipation rate. However, when the SA content is further increased to 1.5 wt%, the critical stretch decreases to 640%. It is speculated that the high viscosity of polymer aggravates the "cage effect" and reduces the free radical efficiency [34], which severely affects the polymerization efficiency of AM monomers and weakens the mechanical properties of the hydrogel.

The surface functional groups on MXene would behave as the crosslinking center to bond with the polymer matrix, which could effectively enhance the stretchablity and mechanical strength of the hydrogel [35]. In Fig. 2b, effects of the MXene contents on the mechanical property of the hydrogel are presented. With the addition of a small amount of MXene (0.5%), the critical stretch of the hydrogel increases dramatically from 860% to 2110%. When the MXene content is increased to 1%, an enhanced critical stretch of 3150% is acquired. However, when higher concentration of MXene (1.5 wt %) is further utilized, the stretchability reduces to 1780%. It suggests that the MXene would absorb free radial on the surface to behave as the center of the crosslinking reaction [35]. The entangled, flexible long chains formed between the nanosheets will move along with the sliding of the nanosheets under tension, effectively enhancing the stretchability and conductivity of the hydrogel. In addition, the multiple functional groups on the surface of the MXene nanosheets could also form substantial hydrogen bonds with the SA-PAM network, to further improve the mechanical strength. Studies based on MXene have reached consensus that the nanofillers in polymer matrix could rapidly dissipate energy and eliminate stress concentration, thus

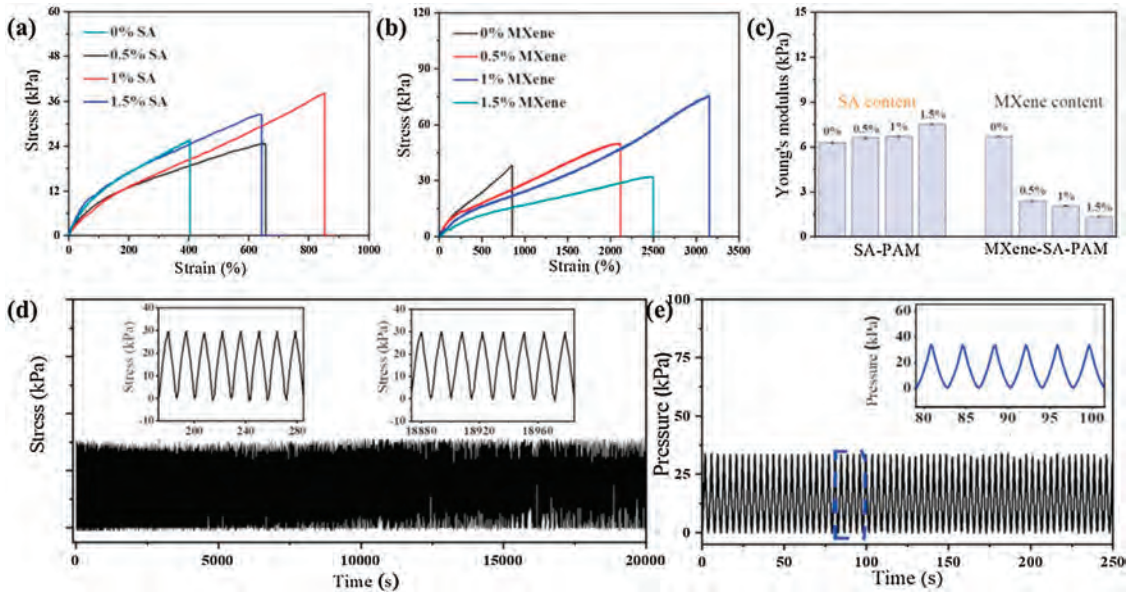

Fig. 2. (a) Stress-strain curves of the hydrogels with different SA loadings (0, 5, 10 and 15 mg/mL). (b) Stress-strain curves of the hydrogels with different MXene loadings (0, 5, 10 and 15 mg/mL). (c) Relationship between tensile Young's modulus of hydrogel with different contents of SA and MXene. (d) The durability test of MXene hydrogel-based strain sensor at the tensile strain of 1600% for more than 1000 cycles. (e) The durability test of MXene hydrogel-based strain sensor at the compression deformation of 50% for 100 cycles.

enhancing the tensile performance [35–38]. However, with excess MXene addition, it will destroy the integrity of the polymer network and shorten the average length of the polymer chains between MXene, resulting in significant reduction in elongation at break.

Despite the fact that certain SA and MXene both have positive influence on the stretchability of the hydrogel, it is noteworthy that SA and MXene has totally different effects on the toughness of the hydrogels. As shown in Fig. 2c, the tensile Young's modulus of the hydrogels increases slightly with the increase of SA content, while decreases significantly with increasing MXene content. It is demonstrated that hydrogen bonding between SA and PAM can reinforce the toughness of the single-networked PAM hydrogel and form robust double-networked hydrogels. For MXene, it will reduce the amount of free radial in the solution, advance the chain termination during the free radical polymerization and reduce the degree of polymerization of PAM, thus depressing the Young's module of the hydrogel. The compression test (Fig. S2 in Supporting information) also reveals that the modulus of the hydrogel decreases with the addition of MXene, and the hydrogel can be easily knotted (Fig. S3 in Supporting information). Therefore, the optimal content of 1% SA and 1% MXene is designated for subsequent tests.

The MXene-composited hydrogel is mechanical robust to tolerate extended cyclic compression and tension test. As displayed in Fig. 2d and e, the mechanical strength of the MXene-based hydrogel maintains stable with nearly 1000 cycles at a tensile strain of 1600% and a compression deformation of 50%, exhibiting a predominant durability and stability. It is mainly due to the "pinning effect" of MXene nanosheets [39]. When the generated microcracks during reproducible cycling tests encounter hard MXene nanosheets, the cracks pinning and deflect, which effectively impedes the continuous microcracks propagation and ensures the hydrogel with excellent anti-fatigue property. Its fatigue resistance in terms of electromechanical performance has been verified, as shown in Fig. S4 (Supporting information).

The electromechanical performances of the hydrogels are evaluated by an intelligent data acquisition device including a computer-controlled dynamic positioning system (ESM303, Mark-10) and a semiconductor characterization analyzer (Keithley 4200-SCS). Sensitivity is a key parameter to evaluate the promising application for strain sensors, and GF, which is defined as $GF = (\Delta R/R_0)/\varepsilon$, is utilized to quantitatively assess the sensitivity, where R_0 is the initial resistance, ΔR is the changes in resistance and ε represents the applied strain. In Fig. 3a, the sensitivity of the SA-PAM and MXene-SA-PAM hydrogels are clearly compared, and an obvious improvement of sensitivity can be distinguished. The GF curves of MXene-SA-PAM hydrogel can be divided into 3 regions, the GF is 3.08 in the initial strain range of 0∼35%, and it increases to 9.17 during 35%∼96% strain, and finally rises to 18.15 with the further increasing strain. In comparison, the SA-PAM hydrogel demonstrates depressed GF, and the GF values 1.08 and 1.84 in the strain range of 0∼35% and 35%∼150%, respectively.

The underlying mechanism of the discrepancy in sensitivity for the two kinds of hydrogels is closely correlated with the high aspect ratio structure and excellent electrical conductivity in MXene. The conductivity of hydrogel is mainly attributed to the localized directional conduction of ions in the aqueous solutions and electron transport of conductive nanoparticles [40]. Figs. 3g–k depicts the stacking status of the MXene to simulate the evolution of conductive network in the hydrogels under tension. In the initial static state without external force (Fig. 3g), the MXene nanosheets in the hydrogel matrix are randomly distributed, and a face-to-edge connection between adjacent nanosheets forms a 3D conductive network. When a tiny tensile force is applied, the connection of the nanosheets converts into edge-to-edge (Fig. 3h). With adequate electron conductive path and decreased contact area, an inferior GF is obtained. After the hydrogel is further stretched, partial conductive joints of MXene nanosheets break and the tunneling effect from the incorporated conductive nanoparticles dominate the electron conductive path (Fig. 3i), revealing more distinct variation in resistance with mild tensile force. With further increment in tension, the tunneling effect of adjacent MXene nanosheets cut off along with expanded spacings, resulting in sharp increase in resistance, and the GF manifests itself with the highest 18.15. In contrast, the SA-PAM displays apparent sluggishness to strains, which is attributed to the constantly maintained ion conduction to external force in the hydrogel. A

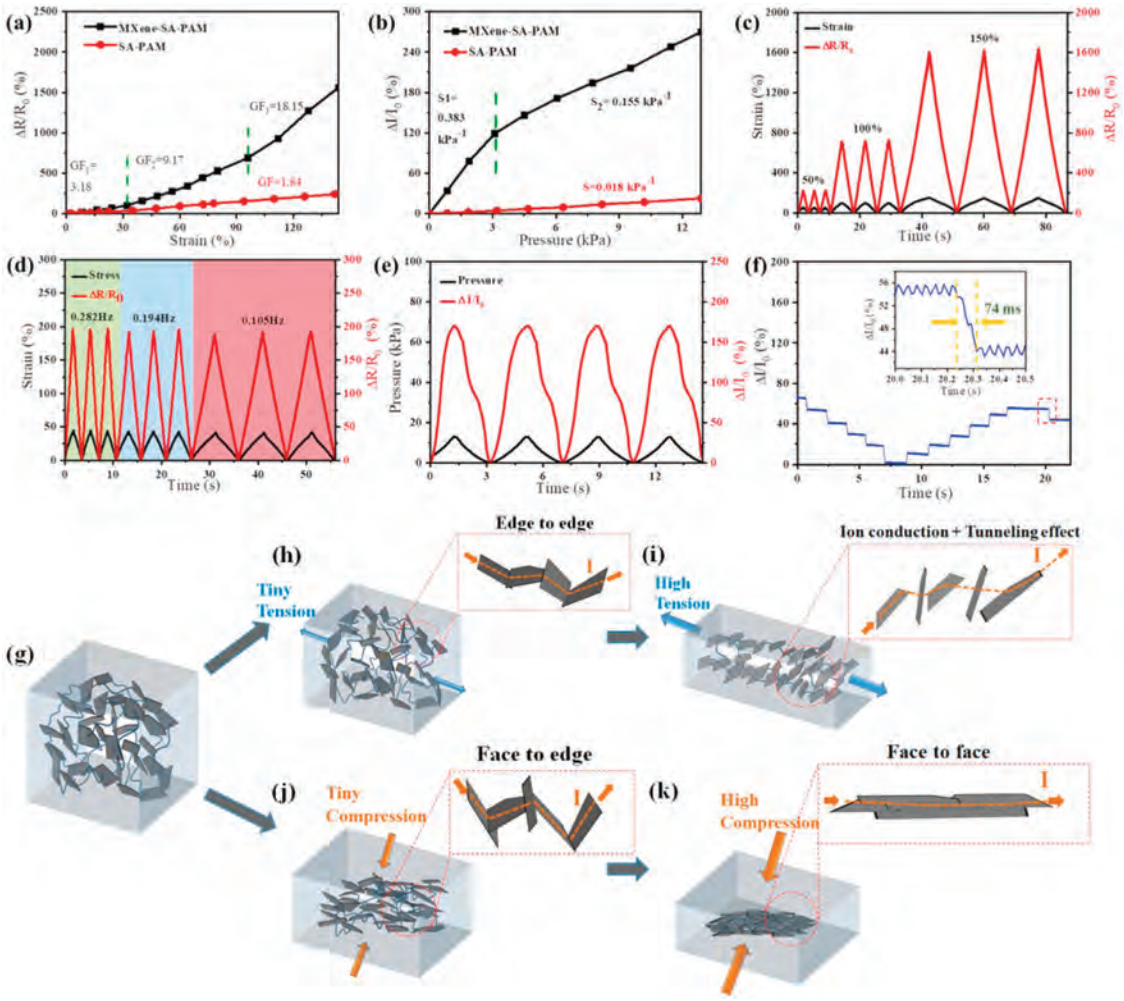

Fig. 3. (a) Relationship between resistance change and strain in a strain sensor. (b) Relationship between current change and stress in a strain sensor. (c) Relative resistance variation as function of time under different tensile strains (50%, 100% and 150%). (d) Frequency-dependent behavior of stress sensors different frequencies (0.282, 0.194 and 0.105 Hz) of % strain. (e) Under a stable cycling pressure (12.8 kPa), the relative current changes with time. (f) Response time of strain sensor when tension changes. Schematic diagram of electromechanical property of MXene-based hydrogel during tensile compression. (g-k) The conversion of conductive path under different strains: (g) no external force, (h) tiny tension, (i) heavy tension, (j) tiny compression, (k) heavy compression.

similar phenomenon related to facial/marginal distribution has been reported [41,42].

The compression sensitivity (S) is also achieved to assess the stress resistance and electrical response to pressure, and $S = \delta(\Delta I/I_0)/\delta P$, where I_0 is the current in the initial state, ΔI is the current change under a certain pressure, and P is the pressure load. Fig. 3b exhibits the current variation to different pressure loading. It can be seen that MXene-SA-PAM hydrogel exhibits a high compression sensitivity of 0.383 kPa^{-1} below 3 kPa, and declines to 0.155 kPa^{-1} in the range of 3∼13.5 kPa. The SA-PAM hydrogel remains a dreadful sensitivity of 0.018 kPa^{-1} in the full pressure range of 0∼13.5 kPa. As can be distinguished from Fig. 3j, the geometry of MXene changes gradually from face-to-edge to face-to-face under tiny compressive deformation, resulting in significant resistance decline in small pressure load (0∼3.0 kPa). When a higher pressure above 3 kPa is applied, the more oriented MXene nanosheets stack into highly dense conductive network (Fig. 3k). With a gentle increase in contact area and limited increase in the numbers of conductive paths, the MXene-based hydrogel reveals a faint compressive sensitivity to higher pressure load. For hydrogel without MXene nanosheets, the Poisson effect of the polymer matrix takes effects and endows the hydrogel low sensitivity to pressure in a wide sensing range.

Fig. 3c shows the resistance response curve of the sensor under different strains. The change of resistance is in close correlation with the variation in strains. The relative resistance variation of the hydrogel under strains of 50%, 100% and 150% are measured to be 222%, 720% and 1610%, which is highly consistent with the results in Fig. 3a. In addition, the resistance response curve coincides with each other in three cycles, suggesting excellent stability and replicability in electrical response. The hydrogel also shows significant electrical response dependence to frequencies. As shown in Fig. 3d, the hydrogel exhibits stable output peak shape under same strain amplitude with different loading rates, which is assigned to the highly crosslinked polymer network and the evenly distributed incorporated MXene nanosheets. Fig. 3e shows the current response curve of the sensor under cyclic compression at a fixed pressure of 12.8 kPa at 0.267 Hz. The current responses transiently to the loading and unloading of pressure, indicating negligible hysteresis in electromechanical performance. Noteworthy, the current response curve of cyclic compression shows inevitable asymmetry, which can be attributed to the inherent viscoelasticity of polymer matrix and the sliding feature of polymer chain between MXene nanosheets. It takes time for the molecular chain to return to its original state when the pressure is removed, which is ascribed to the local curing of the MXene

nanosheets, in terms of bonding with the polymer chains and homogenizing the polymer chain length. The hydrogel also shows a quick response to tension with a response time of 74 ms, as displayed in Fig. 3f, which enables a rapid response to external stimuli and is below than the recent researches [43]. However, the inherent high viscosity of polymer hinders the molecular chain movement under high pressure, resulting in a slower response time of 120 ms (Fig. S5 in Supporting information). Compared with other work, the sensor shows an enhanced stretchability, as well as wider sensing range for electromechanical response (Fig. S6 in Supporting information).

The MXene-based hydrogel, with superior stretchability, sensitivity and durability to external strains and pressures, shows promising application in detections of various human motions. Herein, the hydrogel is packaged into specific scales as a strain sensor and fixed at corresponding epidermis to monitor the human movements from tiny deformations to vibrations. The hydrogel strain sensor could precisely respond to different kinds of human motions with reproducible and durable current outputs. In Fig. S7 (Supporting information), a piece of sensor (20×10 mm) is attached at different fingers to monitor the finger bending. It can be seen that when the finger is bent at a certain angle, the relative currents variation curves display distinct peaks to demonstrate the deformation in knuckles. In addition, different shapes of patterns can be identified when the sensor is attached to the fore, middle, ring and little finger, respectively, indicating accurate tracking of trajectory of different finger movements.

Fig. 4a shows the relative current response to elbows flexion and Fig. 4b displays the electromechanical performance of the strain sensor to shoulder joint motions. Clear and sharp changes in relative current variations are demonstrated, showing accurate response to large-scale human movements. Furthermore, the strain sensor can instruct the discrepancy in movement of muscles and human joints under the same gesture, providing an alternative solution for robot motion capture. In Fig. 4c, the sensor is adhered to the opisthenar and joint separately to indicate the electromechanical performance when making a fist. The relative current variation shows two typical peaks to indicate the deformation and resilience of the joint, while the muscles merely display a single peak wave to explicate the movement. When placed at the eyebrow, distinct rise and decline in relative current variation appears in Fig. 4d, exhibiting promising application for facial expression identification.

Similar and reproducible signal patterns can be clearly distinguished when the sensor was attached to the throat for speech recognition. For the two-syllable "yes", two specific peak shapes reveal (Fig. S8b in Supporting information), while monosyllabic "no" manifests only one peak in the responded current (Fig. S8a in Supporting information). The sensor also can be applied as a flexible touch keyboard for handwriting verification with accurate and repeated response current. When writing "hydrogel" (Fig. S8c in Supporting information), "sensor" (Fig. S8d in Supporting information) and "MXene" (Fig. S8e in Supporting information) on the surface of the sensor with a ballpoint pen, distinguishable and reproducible signal patterns are yielded. It also shows reliable response to the detection of handwriting Arabic numerals 1–9, as displayed in Figs. S8f and S9 (Supporting information).

In summary, by polymerizing MXene nanosheets with AM and SA, an impressive highly stretchable and sensitive hydrogel was obtained. MXene nanosheets constructed strong interaction with the polymer network and provided strong mechanical support for the hydrogel, enabling the MXene-based hydrogel sensors enhanced stretchablity (3150%), robust mechanical strength (Young's Modulus 2.03 kPa^{-1}) and anti-fatigue feature (1000 cycles at 1600% stain with negligible decay). In addition, the highly conductive MXene nanosheets matrix ensured high sensitivity to both tension (GF = 18.15) and compression (S = 0.383 kPa^{-1}) stimuli by autonomously adjusting the contact angel and area among adjacent nanosheet. Moreover, MXene-based hydrogel strain sensors displayed typically dynamic frequency-dependent characteristics and rapid response time of 74 ms with negligible hysteresis in electromechanical performance. In a fabricated strain sensor, the device showed reliable electrical response for body movement detection, voice recognition, facial expression recognition and handwriting verification, suggesting a widespread prospect in robotics, flexible skin and wearable electronics.

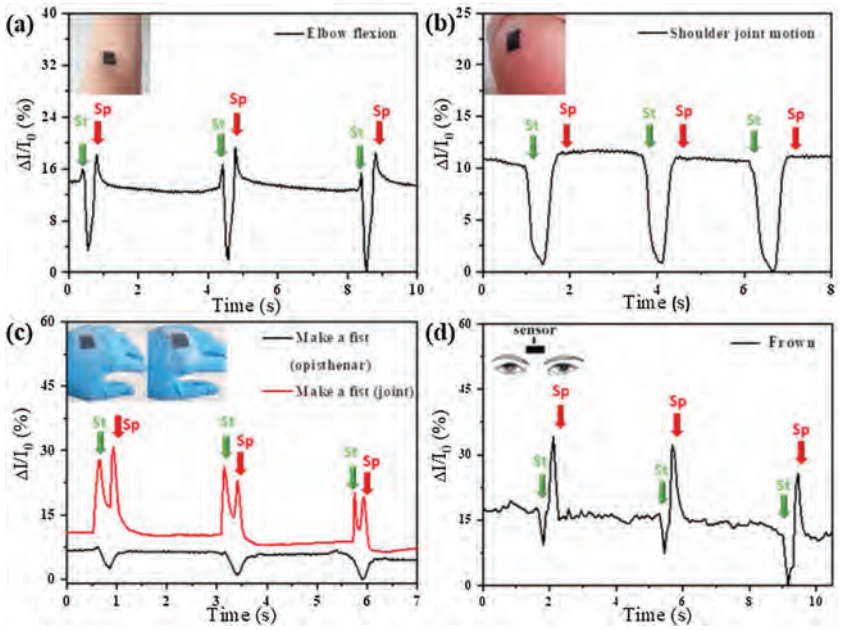

Fig. 4. Photographs of strain sensors used to detect human movement: (a) Elbow flection. (b) Shoulder joint motion. (c) Make a fist. (d) Frown (st: start, sp: stop).

Declaration of competing interest

The authors declare that they have no known competing financial interests or personal relationships that could have appeared to influence the work reported in this paper.

Acknowledgments

The work was supported by the National Natural Science Foundation of China (No. 61775095), six talent peak innovation team in Jiangsu Province (No. TD-SWYY-009), "Taishan scholars" construction special fund of Shandong Province.

Appendix A. Supplementary data

Supplementary material related to this article can be found, in the online version, at doi:https://doi.org/10.1016/j.cclet.2020.12.003.

References

[1] A. Nag, S.C. Mukhopadhyay, J. Kosel, IEEE Sens. J. 17 (2017) 3949–3960.
[2] J. Van Den Brand, M. De Kok, M. Koetse, et al., Solid. Electron. 113 (2015) 116–120.
[3] S. Chandra Mukhopadhyay, IEEE Sens. J. 15 (2015) 1039–1040.
[4] P. Zhu, Z. Zhao, J. Nie, et al., Nano Energy 50 (2018) 744–749.
[5] M. Zhu, N. Inomata, N. Adachi, et al., IEEE Sens. J. 19 (2019) 3626–3632.
[6] H. Wei, C. Tao, Y. Zhu, et al., Appl. Opt. 55 (2016) 2752.
[7] X. Hu, J. Qiu, H. Tan, et al., J. Macromol. Sci. Part A: Pure Appl. Chem. 50 (2013) 983–990.
[8] N. Michida, M. Hayashi, T. Hori, Psychiatry Clin. Neurosci. 52 (1998) 145–147.
[9] X. Zhao, H. Wu, B. Guo, et al., Biomaterials 122 (2017) 34–47.
[10] H. Gao, F. Xiao, C.B. Ching, et al., ACS Appl. Mater. Interfaces 4 (2012) 2801–2810.
[11] Y. Xu, Z. Lin, X. Huang, et al., ACS Nano 7 (2013) 4042–4049.
[12] Z. Lei, Q. Wang, S. Sun, et al., Adv. Mater. 29 (2017) 1700321.
[13] X. Jing, H.Y. Mi, Y.J. Lin, et al., ACS Appl. Mater. Interfaces 10 (2018) 20897–20909.
[14] M. Wang, Y. Chen, R. Khan, et al., Colloids Surfaces A Physicochem. Eng. Asp. 567 (2019) 139–149.
[15] Y. Si, L. Wang, X. Wang, et al., Adv. Mater. 29 (2017) 1700339.
[16] L. Guan, S. Yan, X. Liu, et al., J. Mater. Chem. B Mater. Biol. Med. 7 (2019) 5230–5236.
[17] G. Chen, J. Huang, J. Gu, et al., J. Mater. Chem. A Mater. Energy Sustain. 8 (2020) 6776–6784.
[18] C. Zheng, Y. Yue, L. Gan, et al., Nanomaterials 9 (2019) 937.
[19] H. Gu, H. Zhang, C. Ma, et al., J. Mater. Chem. C Mater. Opt. Electron. Devices 7 (2019) 2353–2360.
[20] J. Lv, C. Kong, C. Yang, et al., Beilstein J. Nanotechnol. 10 (2019) 475–480.
[21] S. Das, F. Irin, L. Ma, et al., ACS Appl. Mater. Interfaces 5 (2013) 8633–8640.
[22] H. Bai, C. Li, X. Wang, et al., Chem. Commun. (Camb.) 46 (2010) 2376–2378.
[23] V.H. Luan, H.N. Tien, L.T. Hoa, et al., J. Mater. Chem. A Mater. Energy Sustain. 1 (2013) 208–211.
[24] L. Qin, G. Ling, F. Peng, et al., J. Colloid Interface Sci. 556 (2019) 232–238.
[25] M. Hu, T. Hu, Z. Li, et al., ACS Nano 12 (2018) 3578–3586.
[26] M. Naguib, V.N. Mochalin, M.W. Barsoum, et al., Adv. Mater. 26 (2014) 992–1005.
[27] Q. Tang, Z. Zhou, P. Shen, J. Am. Chem. Soc. 134 (2012) 16909–16916.
[28] C.J. Zhang, B. Anasori, A. Seral-Ascaso, et al., Adv. Mater. 29 (2017)1702678.
[29] Y.Z. Zhang, K.H. Lee, D.H. Anjum, et al., Sci. Adv. 4 (2018) etta0098.
[30] G. Liu, J. Zou, Q. Tang, et al., ACS Appl. Mater. Interfaces 9 (2017) 40077–40086.
[31] S. Lin, H. Yuk, T. Zhang, et al., Adv. Mater. 28 (2016) 4497–4505.
[32] X. Hu, M. Vatankhah-Varnoosfaderani, J. Zhou, et al., Adv. Mater. 27 (2015) 6899–6905.
[33] W.P. Chen, D.Z. Hao, W.J. Hao, et al., ACS Appl. Mater. Interfaces 10 (2018) 1258–1265.
[34] J.T. Barry, D.J. Berg, D.R. Tyler, J. Am. Chem. Soc. 138 (2016) 9389–9392.
[35] V.N. Mochalin, I. Neitzel, B.J.M. Etzold, et al., ACS Nano 5 (2011) 7494–7502.
[36] Y. Lu, X. Qu, W. Zhao, et al., Research 2020 (2020) 1–13.
[37] W. Zhao, X. Qu, Q. Xu, et al., Adv. Electron. Mater. 6 (2020) 1–9.
[38] G. Ge, W. Yuan, W. Zhao, et al., J. Mater. Chem. A Mater. Energy Sustain. 7 (2019) 5949–5956.
[39] H. Zhang, L. Wang, Q. Chen, et al., Mater. Des. 92 (2016) 682–689.
[40] Z. Song, W. Li, Y. Bao, et al., ACS Appl. Mater. Interfaces 10 (2018) 42826–42836.
[41] G. Wang, W. Huang, N.D. Eastham, et al., Proc. Natl. Acad. Sci. U. S. A. 114 (2017) E10066–E10073.
[42] G. Wang, L.W. Feng, W. Huang, et al., Proc. Natl. Acad. Sci. (2020) 202000398.
[43] H. Liu, M. Li, C. Ouyang, et al., Small 14 (2018) 1801711.